Check for updates

ADVANCED FUNCTIONAL MATERIALS
www.afm-journal.de

Temperature-Induced Effects on Wet-Spun Artificial Spider Silk Fibers

Gabriele Greco, Benjamin Schmuck, Vincenzo Fazio, Giuseppe Puglisi, Giuseppe Florio, Nicola Maria Pugno, Luca Fambri, and Anna Rising**

Silk-based materials are sought after across various industries due to their remarkable properties, including high strength and flexibility. However, their practical application depends largely on how well these properties are maintained under different environmental conditions. Despite significant advancements in the large-scale production of artificial silk fibers, the effects of temperature on their mechanical behavior are understudied. In this study, the mechanical properties of artificial spider silk fibers between −80 and +120 °C are examined and compared to both synthetic and natural silk fibers. The findings reveal that artificial silk fibers maintain their strength up to +120 °C, though the strain at break slightly decreases, remaining above 60%. At −80 °C, the fibers exhibit increased strength, but the strain at break is reduced. While these artificial fibers closely mimic the behavior of natural silk, they show a noticeable reduction in extensibility at low temperatures. Complementing experimental data, differential scanning calorimetry, and thermogravimetric analysis are also conducted, proposing a simple physical model to explain the observed temperature-induced softening. Encouragingly, the degradation temperature of artificial silk is comparable to that of native silkworm and spider silk. This study underscores the importance of enhancing the mechanical robustness of artificial silk to expand its applications.

1. Introduction

The adverse environmental impact of plastic-based materials has catalyzed ongoing research toward the development of new bio-based materials.[1] Spider silk fibers stand out in this regard due to their impressive mechanical properties and environmentally sustainable production methods.[2] These properties stem from the composition of spider silk fibers, which typically consist of multiple proteins that form an amorphous network embedding crystalline regions.[3] If the properties and production method of native silk fibers could be successfully replicated, these materials could have diverse applications across various fields, including biomedicine, soft electronics, optics, and sensor technology.[4–7] The challenge also lies in understanding and maintaining the exceptional properties of silk under varying environmental conditions to ensure their practical utility in these applications.

G. Greco, B. Schmuck, A. Rising
Department of Animal Biosciences
Swedish University of Agricultural Sciences
Box 7023, Uppsala 750 07, Sweden
E-mail: gabriele.greco@slu.se; anna.rising@ki.se

G. Greco, N. M. Pugno
Laboratory for Bioinspired
Bionic
Nano
Meta
Materials & Mechanics
Department of Civil
Environmental and Mechanical Engineering
University of Trento
Via Mesiano, 77, Trento 38123, Italy

The ORCID identification number(s) for the author(s) of this article can be found under https://doi.org/10.1002/adfm.202418435

© 2024 The Author(s). Advanced Functional Materials published by Wiley-VCH GmbH. This is an open access article under the terms of the Creative Commons Attribution License, which permits use, distribution and reproduction in any medium, provided the original work is properly cited.

DOI: 10.1002/adfm.202418435

B. Schmuck, A. Rising
Department of Medicine Huddinge
Karolinska Institutet Neo
Huddinge 141 83, Sweden

V. Fazio, G. Puglisi, G. Florio
Department of Civil Environmental Land Building Engineering and Chemistry
Polytechnic University of Bari
via Orabona 4, Bari 70125, Italy

G. Florio
INFN
Sezione di Bari, Bari I-70126, Italy

N. M. Pugno
School of Engineering and Materials Science
Queen Mary University of London
Mile End Road, London E1 4NS, UK

L. Fambri
Department of Industrial Engineering and INSTM Research Unit
University of Trento
via Sommarive 9, Trento 38123, Italy

16163028, 2025, 15, Downloaded from https://advanced.onlinelibrary.wiley.com/doi/10.1002/adfm.202418435 by Readcube (Labtiva Inc.), Wiley Online Library on [23/04/2025]. See the Terms and Conditions (https://onlinelibrary.wiley.com/terms-and-conditions) on Wiley Online Library for rules of use; OA articles are governed by the applicable Creative Commons License

Materials intended for high-performance applications must retain their properties across a wide range of environmental conditions. Interestingly, silk fibers derived from both spiders and silkworms do not become fragile when exposed to cryogenic temperatures,[8] and display increased tensile strength at low temperatures. Yong et al. studied the mechanical properties of *Bombyx mori* silk fibers across various temperatures and found that fibers tested at −80 °C had up to a 40% increased strength and Young's modulus compared to those tested at room temperature.[9] Conversely, when the temperature exceeded 50 °C, the strength, strain at break, and stiffness of the fibers began to deteriorate, which is due to a transition to a rubbery state.[10,11] A similar pattern was observed by Yang et al., who examined native spider silk from *Trichonephila clavipes*.[12] At low temperatures (−196 °C) spider silk fibers from *Steatoda triangulosa* have 60% increased strength, while the strain at break decreases by 45%, compared to that measured at room temperature.[13] The impressive mechanical properties at low temperatures make silk suitable for applications in cold environments, potentially even for the space industry.[14,15]

Utilizing spiders for industrial-scale silk production is impractical due to the animal's cannibalistic nature.[16] Instead, the field has moved toward developing an artificial mimic of spider silk fibers that can be manufactured on a large scale. Andersson and co-workers proposed an innovative approach to produce artificial spider silk using a miniaturized spider silk protein (mini-spidroin, NT2RepCT).[17] Mini-spidroins are made from globular folded N-terminal and C-terminal domains which flank a short repetitive region. As long as the mini-spidroins are kept natively folded, they can be spun into fibers using exclusively aqueous solutions and a drop in pH, which is similar to how spiders spin their silk.[18–22] An obvious advantage of working with mini-spidroins is that they can be expressed at very high yields.[23,24] In addition, the mechanical properties of the fibers can be tuned by adjusting the spinning parameters,[25,26] and the toughness modulus is comparable to that of native spider silk.[24]

These fibers are therefore interesting from an industrial point of view, but there are currently no available studies on the effects of temperature on the fibers' mechanical properties. To fill this gap, we conducted experiments analyzing the variation of mechanical properties of NT2RepCT fibers across a temperature range from −80 to +120 °C. Additionally, we performed thermogravimetric analysis (TGA) and differential scanning calorimetry (DSC) analyses to better understand the behavior of these fibers under different temperature conditions. Finally, to further support our findings, we also propose a simple physical model to explain the significant impact of temperature on the strength of silk fibers.

2. Results and Discussion

First, a set of control fibers (aramid, silkworm silk, native spider silk) was mechanically characterized across a wide temperature interval in a N_2 atmosphere (**Figures 1** and S1–S4, Supporting Information). We observed a significant increase in strength and strain at break for spider silk at −80 °C, and similarly, silkworm silk fibers exhibited enhanced strength and Young's modulus at −80 °C. An increased temperature (+120 °C) did not induce any significant changes in the fibers' mechanical properties compared to room temperature with the only exception of spider silk that displayed reduced strain at break. These findings are consistent with the existing literature, albeit the previously reported temperature-induced differences in mechanical properties were larger for the natural silks.[9,12] Aramid fibers remained unaffected by temperature variations, also in accordance with previous reports.[27]

Next, we used the same experimental setup to study the mechanical properties of the NT2RepCT fibers. At room temperature (+20 °C) our results align with previously reported data[25,28] (Figures 1 and S4, Supporting Information). At −80 °C, the strength and Young's modulus of the fibers were significantly higher compared to NT2RepCT fibers tested at 20 °C, consistent with findings from studies on silkworm and spider silk[9,12,13] (Figure 1). In addition, within the temperature range of −20 and +120 °C, the strength and Young's modulus of NT2RepCT fibers were not significantly different. The largest negative effect of temperature on the mechanical properties of NT2RepCT fibers was seen for the strain at break and, consequently, the toughness modulus. In particular, a significant decrease of both these parameters was recorded at temperatures higher than 20 °C, consistent with findings reported in the literature for native silk.[9,12,13] Interestingly, contrary to observations on spider silk and silkworm silk, the values of strain at break and toughness modulus of the NT2RepCT fibers tested at temperatures lower than 4 °C were significantly smaller compared to those tested at room temperature (Figures S1, S2, S4, Supporting Information).

Our experiments indicate that artificial spider silk fibers retain their strength across a broad temperature spectrum. However, their strain at break decreases with moderate temperature changes from room temperature. These experiments were performed in a N_2 atmosphere at all temperatures tested (see Materials and Methods), which is likely to reduce the water content in the fibers. Therefore, water content does not appear to be the primary cause of the reduced strain at break at lower temperatures. To further support this hypothesis, we conducted an experiment in a N_2 atmosphere where the NT2RepCT fibers were heated to 120 °C to remove any potential residual water, then cooled to −80 °C and tested (Figure S4, Supporting Information). The results remained the same, i.e., the fibers were still brittle. Additionally, the mechanical properties of fibers tested at 20 °C in a N_2 atmosphere (Figure 1) were comparable to those tested at 20 °C and 35% RH **Figure(2)**. This aligns with literature suggesting that the mechanical properties of fibers remain unchanged at humidity levels below 45% RH.[29–31] From these considerations we may deduce that the reduction in strain at the break of the fibers at low temperatures is primarily attributed to temperature changes rather than to reduced water content.

To further explore the effects of temperature on NT2RepCT fiber's mechanical properties, we incubated the fibers at different temperatures for 1 h in a freezer or in a heated cabinet and then subjected them to tensile testing at room temperature and ambient conditions (Figures 2 and S5, Supporting Information). We found no significant differences in the strength, strain at break, and toughness modulus of NT2RepCT fibers incubated at different temperatures and tested at room temperature. The only exceptions were observed in Young's modulus for fibers incubated at −80 °C which had an increased Young's modulus, and fibers subjected to a temperature larger than 60 °C which

 © 2024 The Author(s). Advanced Functional Materials published by Wiley-VCH GmbH

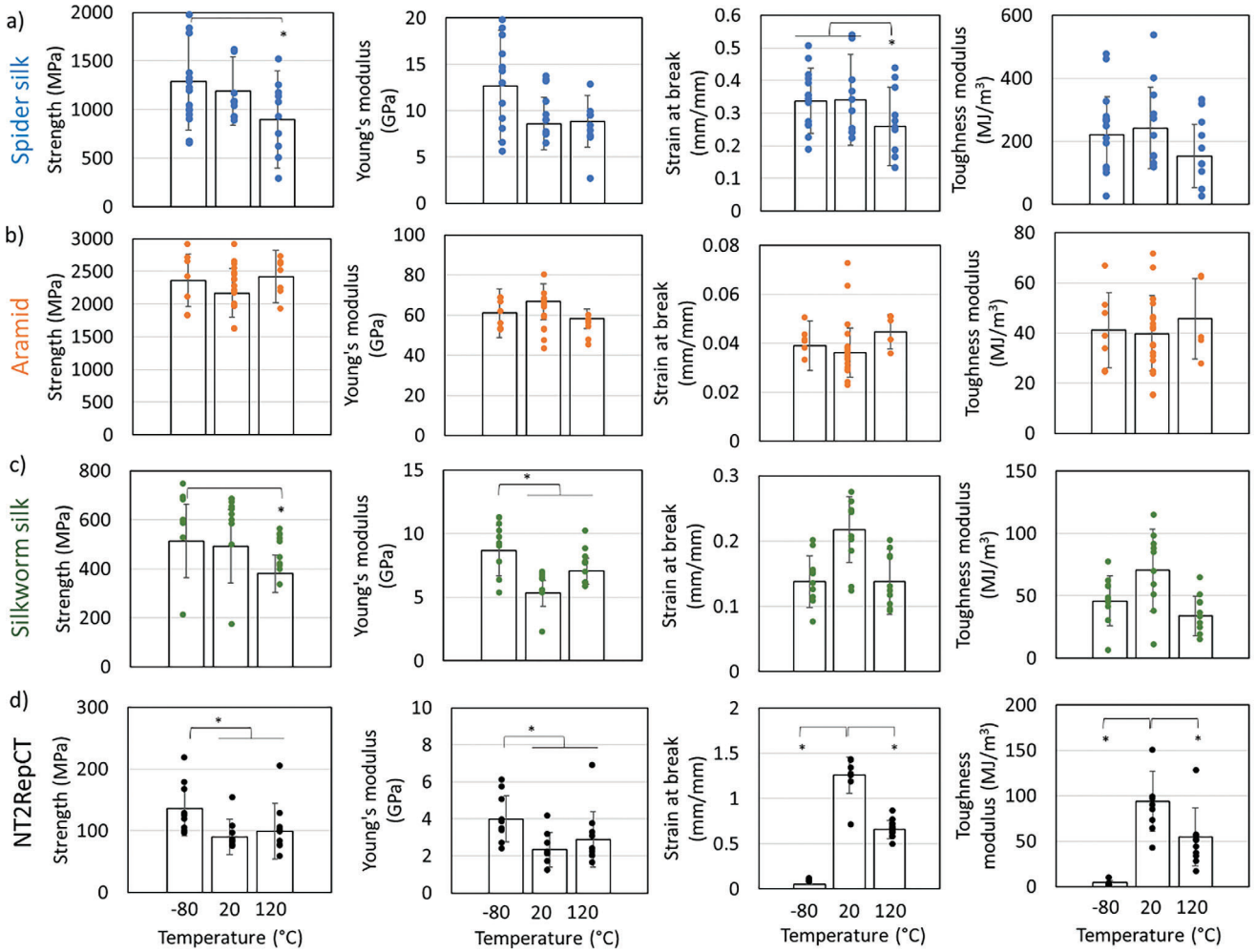

Figure 1. Mechanical properties of a) native spider silk, b) aramid, c) silkworm silk, and d) NT2RepCT fibers at different temperatures in N_2 atmosphere. To see the complete range of temperatures tested for the NT2RepCT fibers, see Figure S5 (Supporting Information).

had a decreased Young's modulus. Overall, the results presented in Figures 1 and 2 support the hypothesis of a reversibility of temperature-induced mechanical properties variations, thus suggesting the potential presence of phase transitions.

To investigate how NT2RepCT fibers respond to high temperatures, we conducted a thermal analysis with TGA (**Figure 3a**; Table S1, Supporting Information). The results were consistent with those of other silk-based materials. Specifically, the water content of artificial silk fibers was estimated to be approximately 10%, similar to that of native silkworm silk fibers, regenerated fibroin films, native spider silk fibers, and recombinant spider silk powder.[32–36] Additionally, the artificial silk fibers exhibited significant degradation above 200 °C, resulting in a residual mass of approximately 50% at 350 °C (complete degradation). This finding is consistent with the reported degradation temperature for spider silk (340 °C)[36] and silkworm silk (317–337 °C).[34] At these critical temperatures (T_c) the strength of silk materials can be presumed to be zero, resembling similar behaviors observed for other biomacromolecules.[37]

In addition to TGA we conducted DSC analysis, as it can offer structural insights and has been employed in various studies on silk.[38,39] Initially, the DSC analysis was conducted on NT2RepCT fibers at a temperature ramp from 20 to 350 °C (Figure 3a). In a second set of experiments, another set of samples was analyzed from 25 to −90 °C, after which the temperature was reversed back to 25 °C, to reflect the conditions under which we determined the mechanical properties of the fibers (Figure 2). The results of the DSC analysis revealed several key findings (Figure 3; Table S2, Supporting Information). There was an initial intense and large endothermic peak observed in the range of 30–120 °C, with a signal at approximately 62 °C, accompanied by a prominent shoulder peak at 75 °C, which is associated with water loss.[40,41] A glass transition peak was univocally identified at 174 °C, in conformity to what has been reported for other silk materials such as pristine silkworm and spider silk fibers, silkworm silk feedstock, fibroin films, and recombinant spider silk powder.[33,36,42–45] The presence of this peak indicates a high mobility of the amorphous regions of the fibers at temperatures around 174 °C.[33,44]

The DSC was also performed at low temperatures to investigate potential reasons for the loss of extensibility observed inartificial silk fibers below 4 °C (Figures S1, S2, and S4, Supporting

© 2024 The Author(s). Advanced Functional Materials published by Wiley-VCH GmbH

16163028, 2025, 15, Downloaded from https://advanced.onlinelibrary.wiley.com/doi/10.1002/adfm.202418435 by Readcube (Labtiva Inc.), Wiley Online Library on [23/04/2025]. See the Terms and Conditions (https://onlinelibrary.wiley.com/terms-and-conditions) on Wiley Online Library for rules of use; OA articles are governed by the applicable Creative Commons License

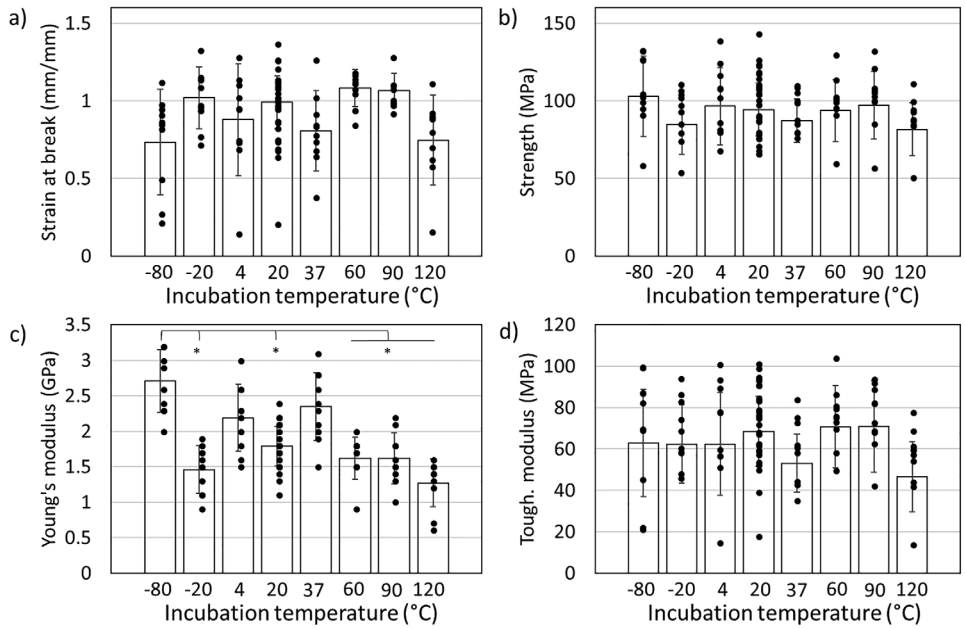

Figure 2. Mechanical properties of the artificial spider silk fibers made from NT2RepCT incubated for 1 h at different temperatures and then tensile tested at room temperature and at 35% RH.

Information). By analyzing the second derivative of the DSC spectra in the temperature range of −80 to 0 °C (Figures 3b and S6, Table S3, Supporting Information), 2 minor signals at −60 and −31 °C, reminiscent of secondary phase transitions likely stemming from a change in mobility of the amorphous regions,[46] could be observed. Interestingly, similar peaks have been documented in previous studies on silk materials. Cunnif et al. and Aparicio-Rojas et al. observed phase-like transitions at −70 and −23 °C respectively, for *Trichonephila clavipes*,[47,48] while Magoshi reported a transition at −40 °C for *Bombyx mori* silk.[49] These types of transitions at lower temperatures were also noted in dynamic thermo-mechanical analysis studies by Torres et al.[10] and Vollrath and Porter,[11] occurring around −70 °C on *Argiope argentata* and *Trichonephila* sp. silks respectively. Vollrath and Porter suggested that these transitions arise from interactions between hydrocarbon side chain groups, albeit without providing further explanations. These low amplitude-phase transitions at low temperatures and the associated reduction in protein mobility could potentially contribute to the observed decrease in extensibility in our artificial silk fibers. To fully understand the mechanisms behind the observed differences in mechanical properties, structural data obtained from X-ray diffraction, IR spectroscopy, and solid-state NMR would be required.[50] However, performing these analyses at very low or high temperatures would necessitate the development of specialized equipment and is beyond the scope of this study. To further elucidate the effects of temperature on the strength of spiders, silkworms, and artificial silk, we employed a straightforward physical model (see Section S1, Supporting Information). This model is based on recent research that analyzes the mechanical behavior of biological macromolecules across various temperatures.[51] The core principle of the model is that thermal fluctuations affect the interactions within and between the proteins, thereby impacting the mechanical properties of the fiber. In particular, at high temperatures, the competition between thermal excitations and elasticity at the molecular scale is such that the effective collective number of interactions

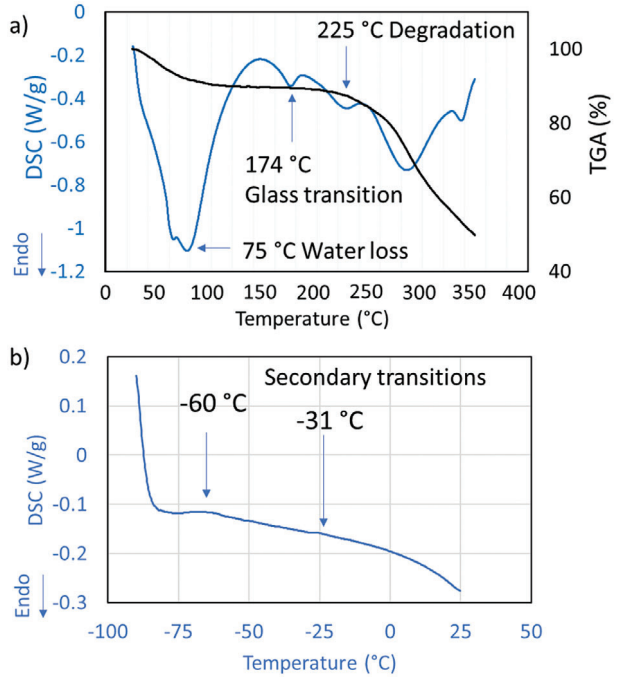

Figure 3. a) DSC (blue) and TGA (black) curves of the artificial spider silk fibers. b) DSC of NT2RepCT silk fibers at low temperatures. TGA and DSC analysis in panel a) were performed with 3.9 and 5.6 mg respectively of NT2RepCT silk. The DSC analysis in panel b) was performed with 5.9 mg of NT2RepCT silk.

© 2024 The Author(s). Advanced Functional Materials published by Wiley-VCH GmbH

16163028, 2025, 15, Downloaded from https://advanced.onlinelibrary.wiley.com/doi/10.1002/adfm.202418435 by Readcube (Labtiva Inc.), Wiley Online Library on [23/04/2025]. See the Terms and Conditions (https://onlinelibrary.wiley.com/terms-and-conditions) on Wiley Online Library for rules of use; OA articles are governed by the applicable Creative Commons License

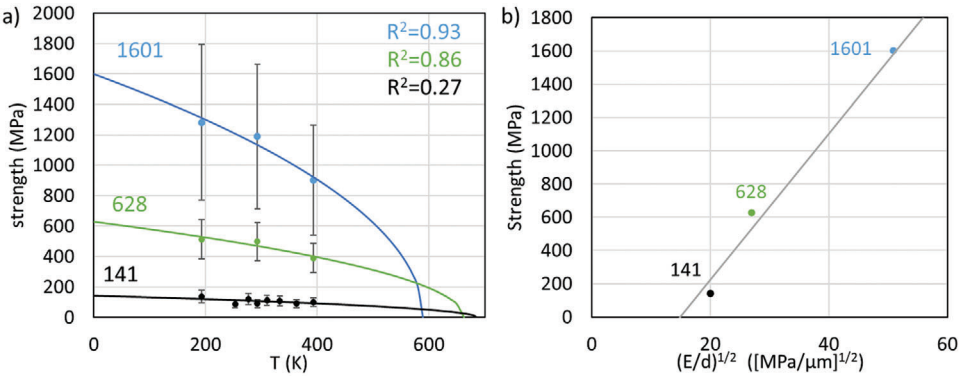

Figure 4. a) Theoretical (continuous lines) versus experimental (dots) strength-temperature curves for spider silk (blue), silkworm silk (green), and artificial NT2RepCT silk fibers (black). The best-fit parameters are $s_0 =$ 1601, 628, 141 *MPa* and $T_c =$ 589, 663, 687 *K* for spider, silkworm, and NT2RepCT silk, respectively. The best-fit values of the critical temperature are compared with experimental data reported in[34,36] in Table 1. b) Comparison of best-fit values of s_0 obtained by the proposed model against theoretical prediction of Porter et al.,[54] The grey line is a linear fit with equation: $y = 44\,x - 658$ and $R^2 = 0.98$. The considered Young's moduli and diameters were the ones measured at −80 °C and are $E =$ 12.67, 8.7, 4 GPa and $d =$ 4.9, 12, 10 μm for spider, silkworm and artificial (NT2RepCT) silk respectively. Note that in this graph the temperatures are expressed in Kelvin (K) and not in Celsius (°C).

decreases. When a critical temperature (T_c) is reached, the material decomposes and the number of interactions becomes negligible, as well as the strength of the material. To correlate the interactions between the protein molecules with the mechanical behavior of the macroscopic fiber, a multiscale analysis was applied.[52,53] From these considerations an analytic relation on the temperature (T) dependent strength (s) of the fiber is determined:

$$s = s\ (T) = s_0 \sqrt{1 - \frac{T}{T_c}} \tag{1}$$

here s_0 is the strength of the fiber at 0 K (−273 °C), i.e., when thermal fluctuations can be neglected. In this context, s_0 and T_c are obtained as best fit parameters of Equation (1). Note that in this model the temperature is expressed in Kelvin (K) and not in Celsius (°C). The numerical simulation based on this model is reported in **Figure** 4a, which shows a good agreement with the experimental data. In Figure S7 (Supporting Information) we also reported the prediction of the model when the values at 253 (−20 °C), 293(20 °C), and 363 K (90 °C) are not included, as for these temperatures the strength did not show the expected monotonic decrease with temperature. Observe that this let us obtain a significantly better prediction of the experimental values also for artificial silks with $R^2 = 0.99$ instead of $R^2 = 0.27$ reported in Figure 4a considering all the experimental points.

In **Table** 1 the predicted (best-fit) values of T_c are compared with experimental data obtained in this work and reported in previous analysis.[34,36] Notice that, unlike s_0, which varies by ≈1000% and 350% between native spider silk and artificial, and silkworm and artificial respectively, T_c is remarkably similar across the 3 types of silk, with only a few percentage points of variation (≈10%). This is consistent with the experimental results and the corresponding errors indicate that the model predicts the critical temperature with satisfactory accuracy. Additionally, these results strongly suggest that the critical temperature of fibers composed of macromolecules does not depend on the number of interactions among and within proteins. To further support the validity of this model, we compare its s_0 prediction with the one made by Porter et al.[54] In this paper, the authors, based on a classical Griffith approach to fracture, show that the material strength is proportional to $(E/d)^{1/2}$, with E and d being Young's modulus and the diameter of the fiber respectively. In general, the model predicts well the values of strength at different temperatures for artificial and natural silk fibers.

An obvious difference between natural silk fibers and NT2RepCT fibers is the molecular weight of the constituent proteins. While natural silks are composed of proteins that can reach several hundreds of kDa in weight,[55] the NT2RepCT protein is only 33 kDa.[17] As a consequence, the intermolecular contacts of the NT2RepCT are likely fewer and the mobility of individual proteins may be higher. This could result in the higher susceptibility to temperature changes observed herein. To counteract this, fibers should probably be spun from recombinant spidroins with a higher molecular weight, which offers a promising direction for future artificial silk fiber production.[56]

Table 1. Comparison between predicted (best-fit) and experimental values of the critical temperature for the 3 different types of silk, with the corresponding difference expressed in percentage.

	T_c [K] Best fit	T_c [K] Experimental	Difference [%]
Spider	589	613	4
Silkworm	663	610	9
Artificial	687	623	10

3. Conclusion

Understanding how materials behave under extreme conditions is essential for identifying suitable applications. This is particularly relevant for biomimetic artificial spider silk, which has not previously been investigated for its temperature dependence. In this study, we present the mechanical properties of NT2RepCT fibers tested across a wide temperature range from −80 to +120 °C and compare them to other natural and synthetic fibers.

© 2024 The Author(s). Advanced Functional Materials published by Wiley-VCH GmbH

16163028, 2025, 15, Downloaded from https://advanced.onlinelibrary.wiley.com/doi/10.1002/adfm.202418435 by Readcube (Labtiva Inc.), Wiley Online Library on [23/04/2025]. See the Terms and Conditions (https://onlinelibrary.wiley.com/terms-and-conditions) on Wiley Online Library for rules of use; OA articles are governed by the applicable Creative Commons License

16163028, 2025, 15, Downloaded from https://advanced.onlinelibrary.wiley.com/doi/10.1002/adfm.202418435 by Readcube (Labtiva Inc.), Wiley Online Library on [23/04/2025]. See the Terms and Conditions (https://onlinelibrary.wiley.com/terms-and-conditions) on Wiley Online Library for rules of use; OA articles are governed by the applicable Creative Commons License

Our findings revealed that the NT2RepCT fibers have superior strength and stiffness at −80 °C compared to the ones measured at ambient conditions, and in addition, retain Young's modulus and strength up to 120 °C. However, the NT2RepCT fibers displayed a lowered strain at break at temperatures lower than 4 °C, which was not observed for the other tested synthetic and natural fiber types. To rationalize these observations, we used results from TGA and DSC experiments and integrated the results with those from the tensile testing to develop a physical model of the material's behavior. Moreover, we conclude that the critical temperature is similar for silkworms, spiders, and artificial silks. Overall, these results underscore the importance of testing and improving artificial silk fibers but also encourage the continued development of artificial silks since they share many of the favorable properties of the native silks. Increased performance of the artificial fibers could potentially be achieved by increasing the molecular weight of the proteins or by adding additional components that are present in the native silk fibers.[3,57,58] This study provides a first step for further innovations in the field of biomimetic materials.

4. Experimental Section

Silkworm Silk, Spider Silk, and Aramid Fibers: Degummed *Bombyx mori* silk cocoons, produced in a controlled environment, were kindly provided by Chul Thai Silk Co., Ltd. (Petchaboon province, Thailand) and degummed as described previously.[59] The aramid fibers used in this study were purchased from Teijin (Technora T240_440). The spider silk was collected from adult females' specimens of *Larinioides sclopetarius* at a constant extrusion rate of 1 cm $^{-1}$s.

Wet-Spinning of Artificial Spider Silk Fibers: The minispidroin NT2RepCT was expressed with *E. coli* in a fed-batch cultivation using a bioreactor and natively purified using chromatographic methods, exactly as previously described.[23] The minispidroins were spun into artificial silk fibers according to an optimized protocol.[25] Briefly, the natively purified and concentrated NT2RepCT in 20 mM Tris HCl buffer (pH8) was stored at 300 mg mL^{-1} in a 1 mL syringe. This spinning dope was extruded through a series of silicon tubings connected to a glass capillary with an orifice diameter of 57 ± 7 µm into a spinning bath containing 0.75 M acetate, pH5, using a flow rate of 17 µL min^{-1}. The fibers were collected at the end of a 80 cm long bath on a wheel rotating at 59 cm s^{-1}. The as-spun fibers were stored in a low-humidity environmental chamber at RH of 10%.

Mechanical Testing: The fibers were mounted on aluminum frames with an opened square 1 × 1 cm window (gauge length around 1 cm). Double-sided tape and glue were used to secure the fibers on the frames. These frames were mounted on a Modular Force Stage (Linkam) device, where the temperature was controlled between −80 and 120 °C in a N_2 atmosphere. Before the testing, the temperature was set and the fibers were incubated for 10 min. The diameter of the fiber was measured before the testing at the desired temperature by placing the Linkam device under an Eclipse TE300 (Nikon) inverted microscope equipped with a DFK DFKNME33UX264 2.3 MP camera and a CFI Plan Fluor DL-10X objective. The mechanical tests of the fibers at room temperature were done using a single-column 5943 tensile tester (Instron) equipped with a 5N load cell. To measure the fiber diameters at room temperature, a Eclipse Ts2R-FL (Nikon) with a DFKNME33UX264 5 MP camera and a CFI Plan Fluor DL-10X objective was used. All the diameters were obtained by averaging 5 measurement points. Then the average diameter was used to calculate the engineering stress by assuming the shape of the cross-sectional area of the fiber was circular. The real cross-section of the fibers was not circular, which means that the engineering stress can be considered underestimated.[60] Engineering stress and engineering strain were used to obtain the tensile strength, Young's modulus (slope of the linear fit in the first 2% of deformation), and the toughness modulus as the area under the stress-strain curve. All the samples were tested at a strain rate of 6 mm min^{-1}.

Differential Scanning Calorimetry (DSC): Calorimetry was performed by using a DSC30 Differential Scanning Calorimeter (Mettler Toledo). Samples of about 15 mg were tested in nitrogen flow of 100 mL mi^{-1}n in the range 30–350 °C at a heating rate of 10 °C min^{-1}. DSC experiments were performed with 5.6 mg of NT2RepCT silk. The DSC experiments performed at low temperatures were done with 5.9 mg of NT2RepCT silk. All the samples were conditioned for 6 days in humidity-controlled conditions prior to the analysis. To assign the temperature of the inflection points at low temperatures, the second derivative of the obtained spectra was used.

Thermogravimietric Analysis (TGA): Thermal degradation was performed in an inert atmosphere by using a TG50 thermogravimetric balance (Mettler Toledo) with a sensitivity of 10^{-3} mg. Each sample had a mass of about 7–10 mg and was tested in alumina crucible flushing nitrogen at 150 mL mi^{-1}n in the range 25–700 °C at a heating rate of 10 °C min^{-1}. TGA experiments were performed with 3.9 mg of NT2RepCT silk.

Supporting Information

Supporting Information is available from the Wiley Online Library or from the author.

Acknowledgements

G.G. and B.S. contributed equally to this work. This work was supported by European Research Council (ERC) under the European Union's Horizon 2020 research and innovation program (grant agreement No 815357), the Center for Innovative Medicine (CIMED) at Karolinska Institutet and Stockholm City Council, Karolinska Institutet SFO Regen (FOR 4–1364/2019), FORMAS (2019-00427, 2023-01313, and 2023-00871), Olle Engkvist stiftelse (207-0375 and 233–0334) and the Swedish Research Council (2019-01257). A.R. and G.G. were supported by Wenner-Gren stiftelse (UPD2021-0047). V.F., G.F. G.P.'s research was funded by the European Union (EU) – Next Generation EU. G.P and G.F. were supported by PNRR, National Center for HPC, Big Data and Quantum Computing – M4C2 – I 1.4 (grant number N00000013, CUP D93C22000430001) – Spoke 5. G.P. and V.F were supported by the PRIN, financed by EU – Next- GenerationEU – National Recovery and Resilience Plan – NRRP – M4C2 – I 1.1, CALL PRIN 2022 PNRR D.D. 1409 14-09-2022 – (Project P2022KHFNB, CUP D53D23018910001) granted by the Italian MUR. G.P. was supported by the PRIN, financed by Eu – Next- Generation EU – NRRP – M4C2 – I 1.1, CALL PRIN 2022 D.D. 104 02-02-2022 – (Project 2022XLBLRX, CUP D53D23006020006) granted by the Italian MUR. G.F. was supported by the PRIN, financed by EU – Next-Generation EU – NRRP – M4C2 – I 1.1, CALL PRIN 2022 PNRR Project P2022MXCJ2, CUP D53D23018940001 and project 2022MKB7MM, CUP D53D23005900006, granted by the Italian MUR. N.M.P. was supported by the European Commission under the FET Open "Boheme" grant no. 863179. N.M.P. acknowledge the financial support of the EU- Next Generation EU – NRRP Missione 4 Componente 2, Investimento N. 1.1, Bando PRIN 2022 D.D. 104/ 02-02-2022 – (PRIN 2022 2022ATZCJN AMPHYBIA) CUP N. E53D23003040006. The authors acknowledge Mrs. Claudia Gavazza for TGA and DSC measurements. G.G. was supported by the project "EPASS" under the HORIZON TMA MSCA Postdoctoral Fellowships – European Fellowships (project number 101103616). A.R. was supported by Horizon 2020 research and innovation program (grant agreement No 815357). B.S. was supported by FORMAS (2023-00871). B.S. was supported by the Swedish Research Council for Sustainable Development, FORMAS (grant number 2023-00871). G.G. was supported by the project "EPASS" under the HORIZON TMA MSCA Postdoctoral Fellowships – European Fellowships (project number 101103616).

Conflict of Interest

The authors declare no conflict of interest.

 © 2024 The Author(s). Advanced Functional Materials published by Wiley-VCH GmbH

Author Contributions

G.G. and A.R. performed conceptualization. G.G., B.S., and L.F. performed Methodology. G.G., B.S., L.F., V.F., N.M.P., G.P., and G.F. performed Investigation. G.G., N.M.P., A.R., and B.S. performed funding acquisition. G.G. and A.R. performed supervision. G.G., B.S., and A.R. wrote the original draft. G.G., B.S., L.F., V.F., G.P., G.F., N.M.P., and A.R. wrote, reviewed, and edited the original draft.

Data Availability Statement

The data that support the findings of this study are available in the supplementary material of this article.

Keywords

aramid fibers, bio-based fibers, phase transition, silkworm silk, wet spinning

Received: September 30, 2024
Revised: October 29, 2024
Published online: November 17, 2024

[1] R. Geyer, J. R. Jambeck, K. L. Law, *Sci. Adv.* **2017**, *3*, 25.
[2] K. Arakawa, N. Kono, A. D. Malay, A. Tateishi, N. Ifuku, H. Masunaga, R. Sato, K. Tsuchiya, R. Ohtoshi, D. Pedrazzoli, T. Ichikawa, S. Fujita, M. Fujiwara, M. Tomita, S. J. Blamires, *Sci. Adv.* **2022**, *6043*, 1.
[3] A. D. Malay, H. C. Craig, J. Chen, N. A. Oktaviani, K. Numata, *Biomacromolecules* **2022**.
[4] A. Dellaquila, G. Greco, E. Campodoni, M. Mazzocchi, B. Mazzolai, A. Tampieri, N. M. Pugno, M. Sandri, *J. Appl. Polym. Sci.* **2020**, *137*, 1.
[5] F. Spizzo, G. Greco, L. Del Bianco, M. Coïsson, N. M. Pugno, *Adv. Funct. Mater.* **2022**, 1.
[6] K. Hey Tow, D. M. Chow, F. Vollrath, I. Dicaire, T. Gheysens, L. Thevenaz, *J. Light. Technol.* **2017**, *8724*, 1.
[7] J. N. Monks, B. Yan, N. Hawkins, F. Vollrath, Z. Wang, *Nano Lett.* **2016**, *16*, 5842.
[8] C. Fu, Y. Wang, J. Guan, X. Chen, F. Vollrath, Z. Shao, *Mater. Chem. Front.* **2019**, *3*, 2507.
[9] Y. Yong, C. Xin, Z. Ping, Y.-H. Wen, S. Zheng-Zhong, *Chem. J. CHINESE Univ.* **2001**, *22*, 1592.
[10] F. G. Torres, O. P. Troncoso, C. Torres, W. Cabrejos, *Mater. Sci. Eng. C* **2013**, *33*, 1432.
[11] F. Vollrath, D. Porter, *Soft Matter* **2006**, *2*, 377.
[12] Y. Yang, X. Chen, Z. Shao, P. Zhou, D. Porter, D. P. Knight, F. Vollrath, *Adv. Mater.* **2005**, *17*, 84.
[13] E. M. Pogozelski, W. L. Becker, B. D. See, C. M. Kieffer, *Int. J. Biol. Macromol.* **2011**, *48*, 27.
[14] A. A. Basheer, *Aircr. Eng. Aerosp. Technol.* **2020**, *92*, 1027.
[15] A. P. Mouritz, *Introduct. Aerospace Mater.* **2012**.
[16] R. Foelix, *Biol. Spider* **2011**, *53*.
[17] M. Andersson, Q. Jia, A. Abella, X. Y. Lee, M. Landreh, P. Purhonen, H. Hebert, M. Tenje, C. V. Robinson, Q. Meng, G. R. Plaza, J. Johansson, A. Rising, *Nat. Chem. Biol.* **2017**, *13*, 262.
[18] X. Li, X. Qi, Y. M. Cai, Y. Sun, R. Wen, R. Zhang, J. Johansson, Q. Meng, G. Chen, *ACS Biomater. Sci. Eng.* **2022**, *8*, 119.
[19] S. Xu, X. Li, Y. Zhou, Y. Lin, Q. Meng, *Biochimie* **2020**, *168*, 251.
[20] Y. Zhou, A. Rising, J. Johanssons, Q. Meng, *Biomacromolecules* **2018**, *19*, 2825.
[21] W. Finnigan, A. D. Roberts, C. Ligorio, N. S. Scrutton, R. Breitling, J. J. Blaker, E. Takano, *Sci. Rep.* **2020**, *10*, 10671.
[22] J. Chen, A. Tsuchida, A. D. Malay, K. Tsuchiya, H. Masunaga, Y. Tsuji, M. Kuzumoto, K. Urayama, H. Shintaku, K. Numata, *Nat. Commun.* **2024**, *15*, 1.
[23] B. Schmuck, G. Greco, A. Barth, N. M. Pugno, J. Johansson, A. Rising, *Mater. Today* **2021**, 1.
[24] T. Arndt, G. Greco, B. Schmuck, J. Bunz, O. Shilkova, J. Francis, N. M. Pugno, K. Jaudzems, A. Barth, J. Johansson, A. Rising, *Adv. Funct. Mater.* **2022**, *2200986*, 2200986.
[25] B. Schmuck, G. Greco, F. G. Bäcklund, N. M. Pugno, J. Johansson, A. Rising, *Commun. Mater.* **2022**, *3*.
[26] G. Greco, J. Francis, T. Arndt, B. Schmuck, F. G. Bäcklund, A. Barth, J. Johansson, N. M. Pugno, A. Rising, *Molecules* **2020**, *25*.
[27] A. Engelbrecht-Wiggans, F. Burni, E. Guigues, S. Jiang, T. Q. Huynh, Z. Tsinas, D. Jacobs, A. L. Forster, *Text. Res. J.* **2020**, *90*, 2428.
[28] G. Greco, H. Mirbaha, B. Schmuck, A. Rising, N. M. Pugno, *Sci. Rep.* **2022**, *12*, 3507.
[29] G. Greco, T. Arndt, B. Schmuck, J. Francis, F. G. Bäcklund, O. Shilkova, A. Barth, N. Gonska, G. Seisenbaeva, V. Kessler, J. Johansson, N. M. Pugno, A. Rising, *Commun. Mater.* **2021**, *2*, 43.
[30] J. Pérez-rigueiro, R. Madurga, A. M. Gañán-calvo, M. Elices, Y. Tasei, A. Nishimura, H. Matsuda, *Sci. Rep.* **2019**, *9*, 2398.
[31] R. W. Work, *Text. Res. J.* **1977**, *47*, 650.
[32] A. Motta, L. Fambri, C. Migliaresi, *Macromol. Chem. Phys.* **2002**, *203*, 1658.
[33] S. Mazzi, E. Zulker, J. Buchicchio, B. Anderson, X. Hu, *J. Therm. Anal. Calorim.* **2014**, *116*, 1337.
[34] D. Kamarun, K. Omar, F. Z. Yusof, *Adv. Mater. Res.* **2015**, *1134*, 123.
[35] A. T. N. Dao, K. Nakayama, J. Shimokata, T. Taniike, *Polym. Chem.* **2017**, *8*, 1049.
[36] S. Osaki, *Acta Arachnol.* **1989**, *37*, 69.
[37] M. Peyrard, A. R. Bishop, *Phys. Rev. Lett.* **1989**, *62*, 2755.
[38] J. Yao, H. Masuda, C. Zhao, T. Asakura, *Macromolecules* **2002**, *35*, 6.
[39] M. Tsukada, M. Obo, H. Kato, G. Freddi, F. Zanetti, *J. Appl. Polym. Sci.* **1996**, *60*, 1619.
[40] J. Magoshi, S. Nakamura, *J. Appl. Polym. Sci.* **1975**, *19*, 1013.
[41] T. Kameda, M. Tsukada, *Macromol. Mater. Eng.* **2006**, *291*, 877.
[42] K. Agarwal, D. A. Hoagland, R. J. Farris, *J. Appl. Polym. Sci.* **1997**, *63*, 401.
[43] H. Kweon, Y. H. Park, *J. Appl. Polym. Sci.* **2001**, *82*, 750.
[44] C. Holland, N. Hawkins, M. Frydrych, P. Laity, D. Porter, F. Vollrath, *Macromol. Biosci.* **2019**, *19*.
[45] J. Guan, Y. Wang, B. Mortimer, C. Holland, Z. Shao, D. Porter, F. Vollrath, *Soft Matter* **2016**, *12*, 5926.
[46] W. Huang, S. Krishnaji, X. Hu, D. Kaplan, P. Cebe, *Macromolecules* **2011**, *44*, 5299.
[47] P. M. Cunniff, S. A. Fossey, M. A. Auerbach, J. W. Song, D. L. Kaplan, W. W. Adams, R. K. Eby, D. Mahoney, D. L. Vezie, *Polym. Adv. Technol.* **1994**, *5*, 401.
[48] G. M. Aparicio-Rojas, G. Medina-Vargas, E. Díaz-Puentes, *Heliyon* **2020**, *6*, e05262.
[49] J. Magoshi, Y. Magoshi, *J. Polym. Sci.* **1975**, *13*, 1347.
[50] V. S. Bajaj, P. C. A. Van Der Wel, R. G. Griffin, *J. Am. Chem. Soc.* **2009**, *131*, 118.
[51] G. Florio, G. Puglisi, *Acta Biomater.* **2023**, *157*, 225.
[52] G. Puglisi, D. De Tommasi, M. F. Pantano, N. M. Pugno, G. Saccomandi, *Phys. Rev. E* **2017**, *96*, 19.
[53] V. Fazio, D. De Tommasi, N. M. Pugno, G. Puglisi, *J. Mech. Phys. Solids* **2022**, *164*, 104857.
[54] D. Porter, J. Guan, F. Vollrath, *Adv. Mater.* **2013**, *25*, 1275.
[55] N. A. Ayoub, J. E. Garb, R. M. Tinghitella, M. A. Collin, C. Y. Hayashi, *PLoS One* **2007**, *2*.
[56] B. Schmuck, G. Greco, T. B. Pessatti, S. Sonavane, V. Langwallner, T. Arndt, A. Rising, *Adv. Funct. Mater.* **2023**.
[57] N. Kono, H. Nakamura, M. Mori, Y. Yoshida, R. Ohtoshi, A. D. Malay, *Proc. Natl. Acad. Sci. U.S.A.* **2021**, 1.

© 2024 The Author(s). Advanced Functional Materials published by Wiley-VCH GmbH

16163028, 2025, 15, Downloaded from https://advanced.onlinelibrary.wiley.com/doi/10.1002/adfm.202418435 by Readcube (Labtiva Inc.), Wiley Online Library on [23/04/2025]. See the Terms and Conditions (https://onlinelibrary.wiley.com/terms-and-conditions) on Wiley Online Library for rules of use; OA articles are governed by the applicable Creative Commons License

[58] S. Sonavane, S. Hassan, U. Chatterjee, L. Soler, L. Holm, A. Mollbrink, G. Greco, N. Fereydouni, O. Vinnere Pettersson, I. Bunikis, A. Churcher, H. Lantz, J. Johansson, J. Reimegård, A. Rising, *Sci. Adv.* **2024**, *10*, eadn0597.

[59] L. Del Bianco, F. Spizzo, Y. Yang, G. Greco, M. L. Gatto, G. Barucca, M. Pugno, A. Motta, *Nanoscale* **2022**.

[60] G. Greco, B. Schmuck, S. K. Jalali, N. M. Pugno, A. Rising, *Biophys. Rev.* **2023**, *4*.

© 2024 The Author(s). Advanced Functional Materials published by Wiley-VCH GmbH

16163028, 2025, 15, Downloaded from https://advanced.onlinelibrary.wiley.com/doi/10.1002/adfm.202418435 by Readcube (Labtiva Inc.), Wiley Online Library on [23/04/2025]. See the Terms and Conditions (https://onlinelibrary.wiley.com/terms-and-conditions) on Wiley Online Library for rules of use; OA articles are governed by the applicable Creative Commons License

Supporting Information

Temperature-induced effects on wet-spun artificial spider silk fibers

Gabriele Greco [a,b,&*], Benjamin Schmuck[a,c,&], Vincenzo Fazio[d], Giuseppe Puglisi[d], Giuseppe Florio[d,e], Nicola M. Pugno[b,f], Luca Fambri[g], and Anna Rising[a,c*]

[a] *Department of Animal Biosciences, Swedish University of Agricultural Sciences, Box 7023, 750 07 Uppsala, Sweden*

[b] *Laboratory for Bioinspired, Bionic, Nano, Meta, Materials & Mechanics, Department of Civil, Environmental and Mechanical Engineering, University of Trento, Via Mesiano, 77, 38123 Trento, Italy*

[c] *Department of Medicine Huddinge, Karolinska Institutet, Neo, 141 83 Huddinge, Sweden*

[d] *Department of Civil Environmental Land Building Engineering and Chemistry, Polytechnic University of Bari, via Orabona 4, 70125 Bari, Italy*

[e] *INFN, Sezione di Bari, I-70126, Bari, Italy*

[f] *School of Engineering and Materials Science, Queen Mary University of London, Mile End Road, London E1 4NS, UK*

[g] *University of Trento, Department of Industrial Engineering and INSTM Research Unit, via Sommarive 9, 38123 Trento, Italy*

[&] these authors contributed equally

* Corresponding authors: gabriele.greco@slu.se; anna.rising@ki.se;

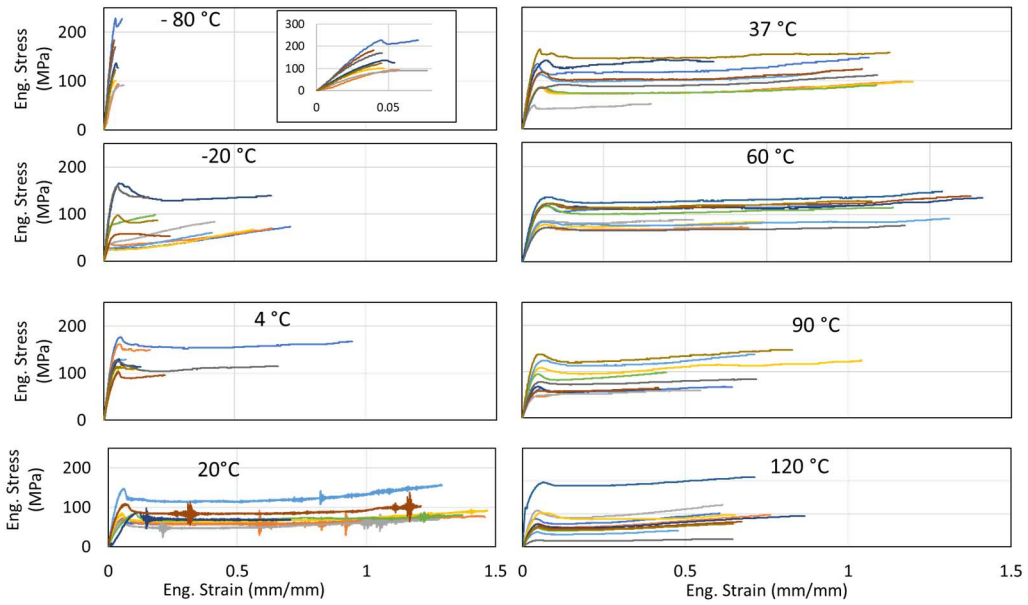

Figure S1: All stress-strain curves of the NT2RepCT fibers tested at different temperatures in N_2 atmosphere.

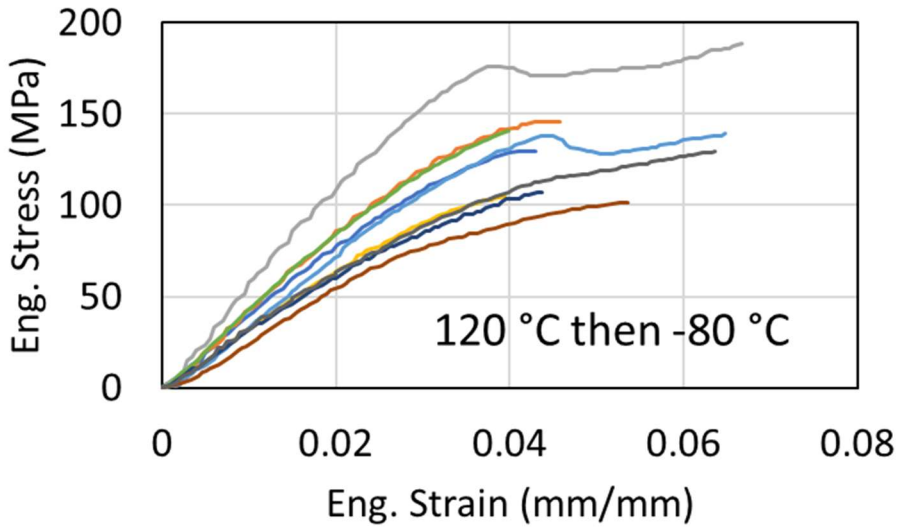

Figure S2: Stress-strain curves of the NT2RepCT fibers warmed up to 120 °C to remove the water and then tested at -80 °C in N_2 atmosphere.

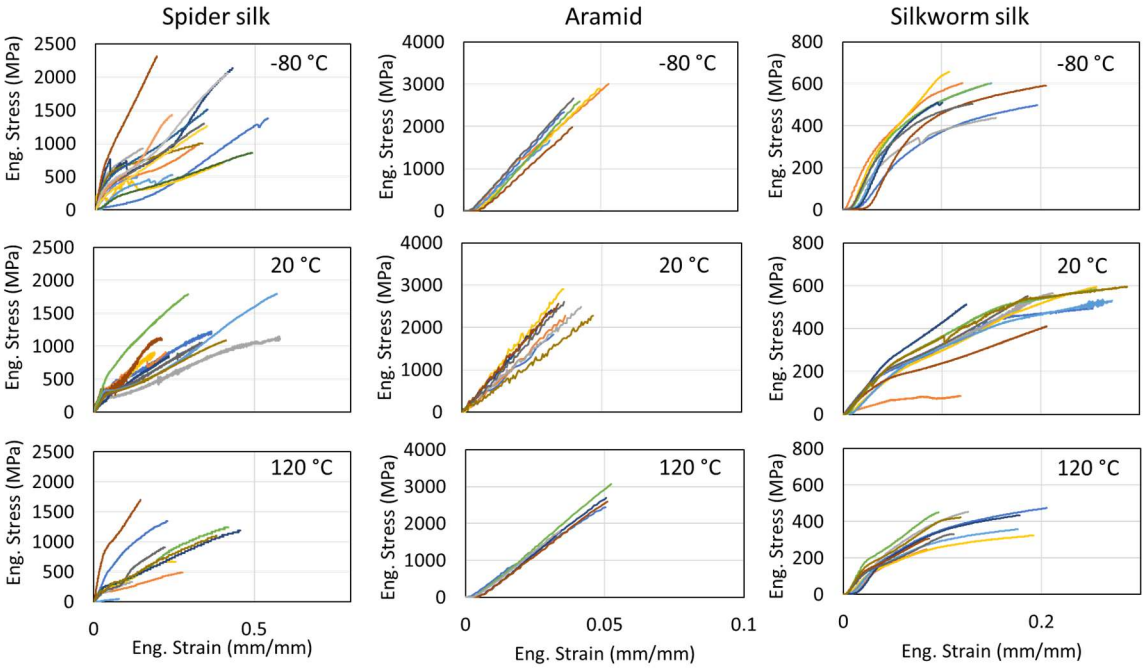

Figure S3: Stress-strain curves of the Spider silk, silkworm silk, and aramid fibers used for comparison at different temperatures in N_2 atmosphere.

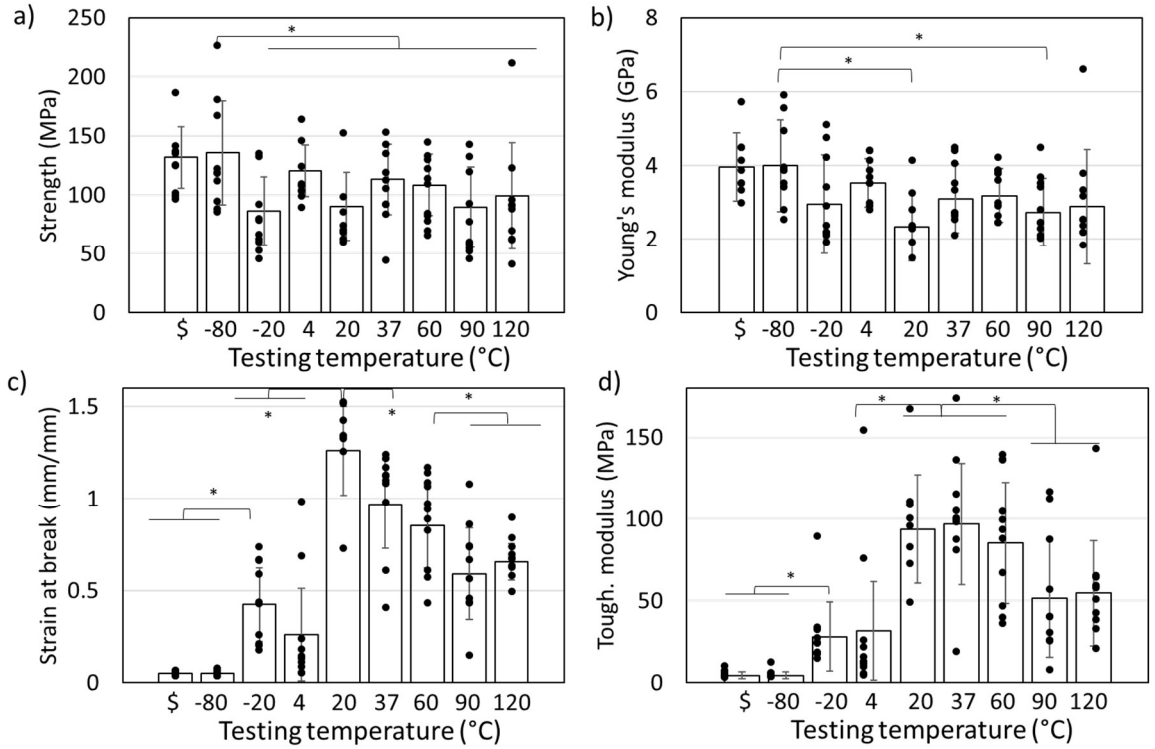

Figure S4: Mechanical properties of the NT2RepCT artificial spider silk fibers tested at different temperatures. The symbol $ on the horizontal axis corresponds to the fibers that were exposed to 120 °C before being tested at -80 °C. All these tests were done in N_2 atmosphere.

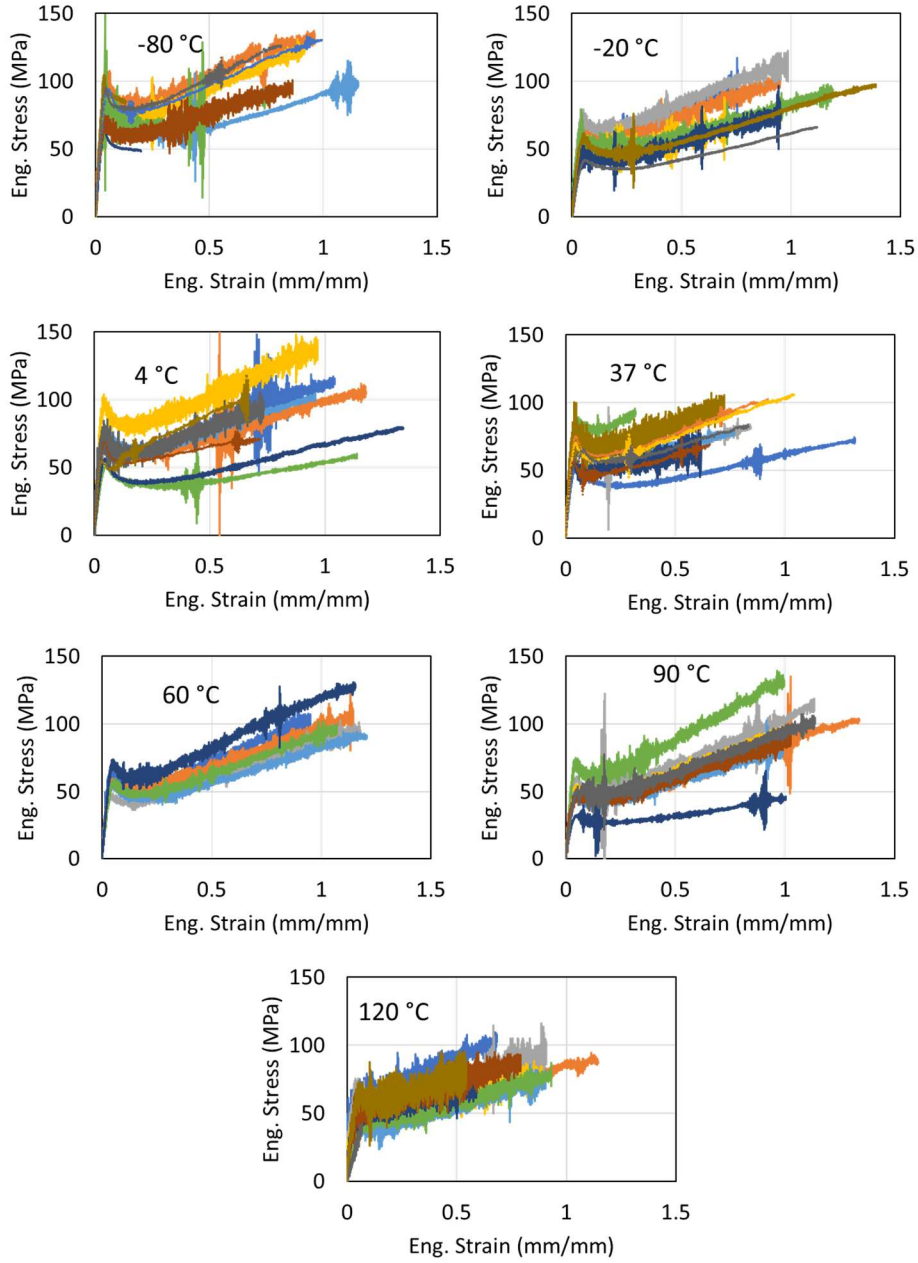

Figure S5: Stress-strain curves of the NT2RepCT fibers that were incubated at different temperatures for 1 hour and then tensile tested at room temperatures at 35% RH.

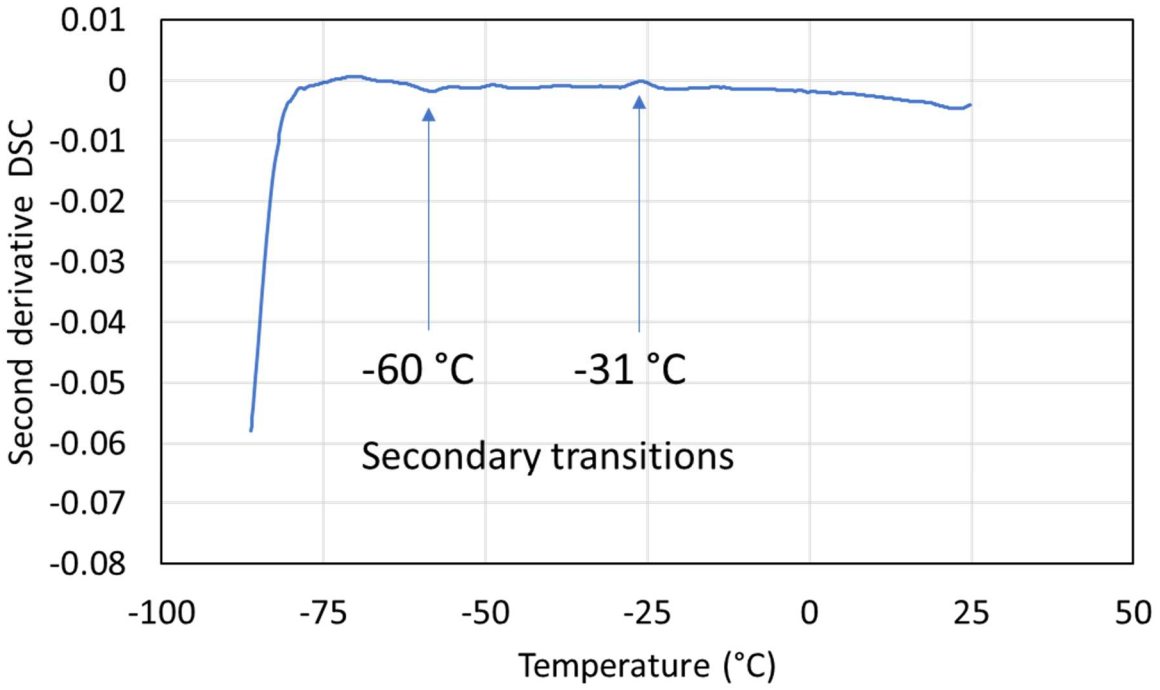

Figure S6: Second derivative of the DSC curve performed at low temperatures (displayed in Figure 3b), which highlights the two inflection points associated to secondary transitions.

Supplementary section S1: the physical model

To support the experimental findings of this work we developed a simple physical model extending the results proposed in Florio & Puglisi[51] to study the significant effect of thermal fluctuations on the mechanical behavior of biological molecules undergoing unzipping. Indeed, both mechanical and thermal softening observed in silks can be mainly ascribed to the protein network bonds effectively weakening and breaking due to the competition between thermal excitations and interactions when the temperature is increased. If such bonds are weakened or broken, it is easier to stretch and unfold the proteins composing the silk, which leads to a decrease of the mechanical properties of the thread. The model developed by Florio & Puglisi[51] allows to deduce that the force measured during the unzipping, overstretching or unfolding of the protein depends on temperature and scales as

$$F = F(T) = F_0\sqrt{1 - \frac{T}{T_c}} \qquad \text{(S1)}$$

where T and T_c are the absolute temperature of the system and a "critical" value of the temperature, respectively, whereas F_0 is the force inducing a conformational transition of the molecules when thermal fluctuations can be neglected ($T \to 0\ K$). In particular, T_c represents a theoretical temperature threshold such that the bonds of the protein network are broken, due to thermal fluctuations only. Here we identify such theoretical value with our experimental

observation (see Fig. 3a) and literature: 350 °C for NT2RepCT fibers, 340 °C for spider silk[36], and 330 °C for silkworm silk[34].

The rigorous extension of this model to the different silk threads requires a complex multiscale analysis that is out of the aim of this paper (see e.g. Fazio et al.[53]). Here, by following previous approaches[52], we assume that in the protein network there are n_s interactions between individual proteins that contribute to the mechanical strength of the fiber and that the observed important difference measured in the macroscopic strength of the different fibers is due to different values of n_s.

By following this simple prototypical model of parallel effective identical macromolecules for the different materials, the strength decreases for increasing temperatures according to the following simple law

$$s = s(T) = n_s\, F(T) = s_0\sqrt{1 - \frac{T}{T_c}} \qquad \text{(S2)}$$

where $s_0 = n_s F_0$ is the strength at $T = 0\ K$.

In Figure 4a we show the curves obtained by best fit for spider silk (blue), silkworm silk (green), and NT2RepCT fibers by using Eq. (1). In Fig. S7 we reported the same comparison with the experimental results when the values at 253, 293, and 363 K are not included. Indeed for these temperatures we do not observe a monotonic decreasing and we may argue that this may depend on the described experimental uncertainty. Observe that thanks to this assumption we obtain a greater predictivity for artificial silks passing from $R^2 = 0.27$ to $R^2 = 0.99$. The critical temperature predicted by the model in this case is T_c = 611 K, with an error with respect to the experimental one decreasing from 10% to 2% (see Table 1).

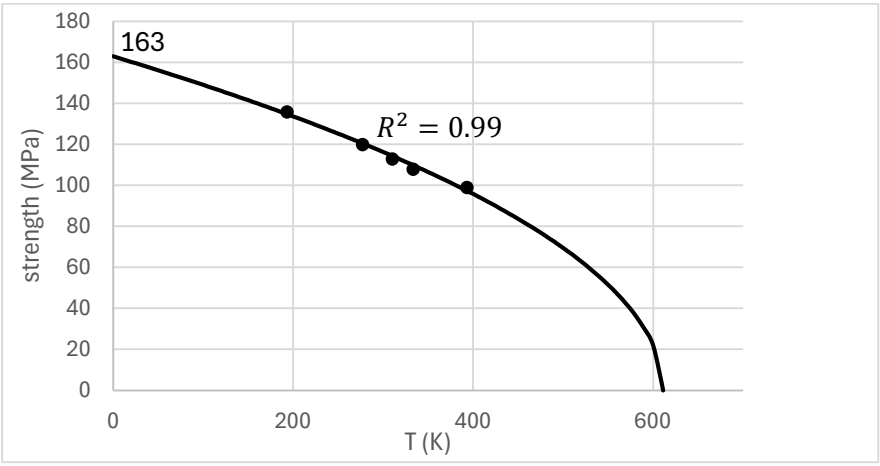

Figure S7: Theoretical (continuous lines) vs experimental (dots) strength-temperature curves for NT2RepCT silk fibers when the temperature values of 253, 293, and 363 K, determining a non-monotonic behavior, are not included.

In Table 1, the values of the critical temperature T_c predicted by the model (obtained as best fit parameters), are compared with those experimentally measured by the TGA analysis for artificial silk (see Fig. 3a) and obtained from literature for spider and silkworm silk[34,36]. As previously described, these values can be considered as critical (denaturation) temperatures after which the material strength decreases to zero. Moreover, natural silks are expected to have higher n_s, i.e., larger number of interactions between individual proteins that contribute to the fiber strength. As a result, s_0 in Equation (S2) is larger for natural silks with respect to artificial silks, in agreement with the experiments.

We remark that the effective number of interactions between individual proteins depends on many complex effects such as spinning rate, network conformation, etc. Here, we simply assume n_s (and, thus, s_0) as a fitting parameter. To support our result, we also compared the values of the best fit parameters with the result in Porter et al[54] assuming that the material strength is proportional to $\sqrt{E/d}$ with E the modulus and d the diameter of the fibers. In Figure 4b we used the experimental (average) values of E and d for the different silks at the temperature $T = -80°\text{C}$ (the lowest temperature with available experimental data) and the values of s_0 obtained from the best fit for the different silks. We obtained a linear trend with $R^2 = 0.98$. Such a comparison gives a further theoretical support to the proposed theoretical framework and validates the efficacy of the model to determine s_0.

Observe that in Florio & Puglisi[51] a clear physical interpretation of T_c is given, depending on the debonding energy of bonds between proteins and the elastic energy of the constituent molecules. In particular, the larger T_c, the lower is the thermal softening effect. Interestingly, the experimental value of T_c in the range of $600\ K$ is significantly larger with respect to other biological materials undergoing unzipping under thermal effects and mechanical stretch such as DNA (with $T_c = 370\ K$), thus explaining the better performance of silks under extreme thermal environment. In particular, T_c grows as the number of bonds per unit of protein length is increased.

Table S1. Results of the TGA analysis of NT2RepCT fiber bundles.

Mass loss 25-150°C	Residual mass at 275°C	Mass loss 150-275°C	Residual mass 350°C	Mass loss 275-350°C	Mass loss 350-700°C	Residual mass at 700°C
-10.29%	77.69%	-12.02%	49.76%	-25.93%	-22.37%	27.39%

Table S2. Results of DSC analysis of NT2RepCT fiber bundles. *intense shoulder peak

Endo peak 1 30-145°C	(J/g)	Endo peak 2 150-190°C	(J/g)	Endo peak 3 200-240°C	(J/g)	Endo peak 4 240-330°C	(J/g)	Onset °C	Loss %
75°C (62°C)*	294	174°C	6.1	225°C	6.7	283°C	73	338	-53%

Table S3. Results of DSC analysis of NT2RepCT fiber bundles at low temperatures (heating step from -90 °C to 25 °C at 10 °C/min).

Inflect. point 1	Inflect. 2
-31 °C	-60 °C